Journal of Aeronautics, Astronautics and Aviation, Vol. 52, No. 1, pp. 63 – 82 (2020)
DOI: 10.6125/JoAAA.202003_52(1).06

Thermophysical Behaviour of Biofuel under Detonation Combustion *

Izham Izzat Ismail **, Muhammad Fadzrulizwan Mohd Yusof, Muhammad Hanafi Azami, and Ahmad Ariffin Mohd Ihsan

Department of Mechanical Engineering, IIUM, Kuala Lumpur, Malaysia and Department of Mechanical & Material Engineering, UKM, Kuala Lumpur, Malaysia.

ABSTRACT

The purpose of this research is to assess biofuel on thrust behaviour and the propulsive performance of ideal Pulse Detonation Engines (PDEs) based on the parametric cycle of analysis for supersonic heat addition. Detonative combustion utilises shocks and detonation waves by providing pressure-rise combustion and prominently result in higher propulsive and thermodynamic efficiency as compared to conventional isobaric heat addition in a Brayton cycle combustor. This research uses the numerical approach to calculate the performance of aircraft by changing the ambient condition. Furthermore, this research chose to study two biofuels; Bioethanol and Babassu Biokerosene BBK100. Both biofuels have been used in the conventional air-breathing engine. The researchers in this study examined the performance of the fuels by observing the pressure, Mach number, temperature, and density ratios. The condition of the mass flux varied from $3500\,kg/sm^{-2}$ to $9400\,kg/sm^{-2}$ while the initial temperature varied from 200K up to 790K, due to the characteristics of Bioethanol and Babassu Biokerosene BBK100, there are differences in detonation velocity, propulsive efficiency, and thermodynamic efficiency. Babassu Biokerosene BBK100 has better detonation velocity as compared to Bioethanol, which is 1900.4 m/s. Hence, the result shows that biofuel is feasible for the Pulse Detonation Engines (PDEs) as it brings due improvement to aircraft performance.

Keywords: Pulse Detonation Engine; Biofuels; Babassu Biokerosene BBK100; Parametric Cycle;

I. INTRODUCTION

The Pulse Detonation Engine (PDE) is a contemporary subject of interest as it has the potential to become the next generation propulsive device for air-breathing engines and rocket propulsion [1,2]. Pulse Detonation Engine (PDE) is an improvement of the pulse-jet engine, so it has some similarities. However, PDEs detonate propellant mixtures to produce higher thrust and efficiency, rather than deflagrate [3,4]. The first introduction to PDEs was in 1940 by Hoffman when he mixed both acetylene and benzene fuels with oxygen [5]. In 1950, scholars Nicholls and Dunlap continued the research by performing a series of experiments for single-cycle and multiple-cycle detonation for hydrogen-oxygen, hydrogen-air, acetylene-oxygen and acetylene-oxygen mixtures in 6-ft (182.9cm) tube [6]. Since then, other researchers have continued to study PDEs, and the interest in PDE as a propulsion system technology has prevalently increased.

According to [7], combustion is defined as an exothermic chemical reaction between a fuel and an oxidiser that, once initiated, can sustain itself for as long as the ingredients are present in the proper proportions and the thermal diffusion do not exceed its limits. Combustion wave velocity is dependent on several factors, including

* Manuscript received, December 6, 2019, final revision, December 7, 2019

** To whom correspondence should be addressed, E-mail: izhamizzatismail@gmail.com

mixture composition, pressure, temperature, and the geometry of the volume where the combustion occurs [8]. Detonation is a supersonic combustion wave that propagates more than a thousand meters per second. Detonation produces more energy and large overpressures than deflagration [9]. As stated in [10], detonation velocity for fuel/air mixtures is usually over 1.8 km/s and creates a high-pressure increase of more than 10 times compared with deflagration. According to [7], in a detonation, the combustion reaction and shock wave propagation proceed in an entirely coupled and mutually supporting manner. The shock charged on the unreacted material by the supersonic combustion wave causes a rapid heating and subsequent combustion of the reactants to sustain the reaction.

On another note, the world would benefit tremendously with the advent of alternative fuels. Hence, in the effort of sustaining the environment, researchers have delved into several alternative fuels such as Jet-A, Acetylene, Jatropha Bio-synthetic Paraffinic Kerosene (JSPK), and Microalgae Biofuel in the one-dimensional numerical analysis [11]. Biofuel is a fuel derived from plant, agricultural and waste products; for example, Ethanol and Biodiesel. With the understanding of the Pulse Detonation cycle, this research applies the combustion of biofuel with oxygen in the detonation cycle. The indispensability of PDEs in flights application has had considerable recognition worldwide.

At the same time, the world is also facing a crisis of energy shortage due to the continuously depleting reserved fossil fuel [12]. Hence, to overcome this issue, scientists need to find a biofuel suitable for the PDEs cycle to resolve the said environmental issue. Nevertheless, would the biofuels used in PDEs surpass the conventional fuel in aircraft performance?

II. RANKINE-HUGONIOT CURVE

The Rankine-Hugoniot curve represents the solution to any steady-state combustion wave. The study on detonation waves in engine performance is somewhat reasonable since the significant changes in the fluid properties occur over very short distances [2]. By assuming that the flow is steady, adiabatic, and one-dimensional, and neglecting body forces, the models describe the fundamental physics of simple one-dimensional detonations in a constant area duct. The analysis is based on the equations of conservation for mass, momentum, and energy across the detonation, and the equation of state. Combining the continuity and momentum equations yields the following:

$$(\rho_1 u_1)^2 = (\rho_2 u_2)^2 = m^2 = -\frac{P_2 - P_1}{v_2 - v_1} \quad (1)$$

$$\frac{\gamma}{\gamma - 1}\left(\frac{P_2}{\rho_2} - \frac{P_1}{\rho_1}\right) - \frac{1}{2}(P_2 - P_1)\left(\frac{1}{\rho_2} - \frac{1}{\rho_2}\right) = q \quad (2)$$

Where the equivalences are as follows:

1: unburned gas upstream of the detonation wave.
2: burned gas immediately downstream of the detonation wave.
ρ = density
u = one-dimensional velocity
m= mass (kg)
q = heat addition (per unit mass)
v = specific volume = 1/ρ
γ = heat capacity ratio (1.4)

Since $(\rho_1 u_1)^2$ and $(\rho_2 u_2)^2$ are always positive, the terms $(P_2 - P_1)$ and $(v_2 - v_1)$ must be the opposite sign. Table 1 displays two combustion processes, deflagration and detonation. Equation 1 represents the Rayleigh-line relation and Equation 2 represents the Rankine-Hugoniot relation.

Table 1 Combustion process, as indicated by the Rayleigh Line.

Combustion process	ΔP	Δv
Deflagration	Negative	Positive
Detonation	Positive	Negative

The Rankine-Hugoniot relation denotes the possible solutions of pressure and density values of the combustion products. Whereas, the Hugoniot curve is defined by the relationship between enthalpy (h), pressure (P), and density (ρ) of the gases in a combustion event [7].

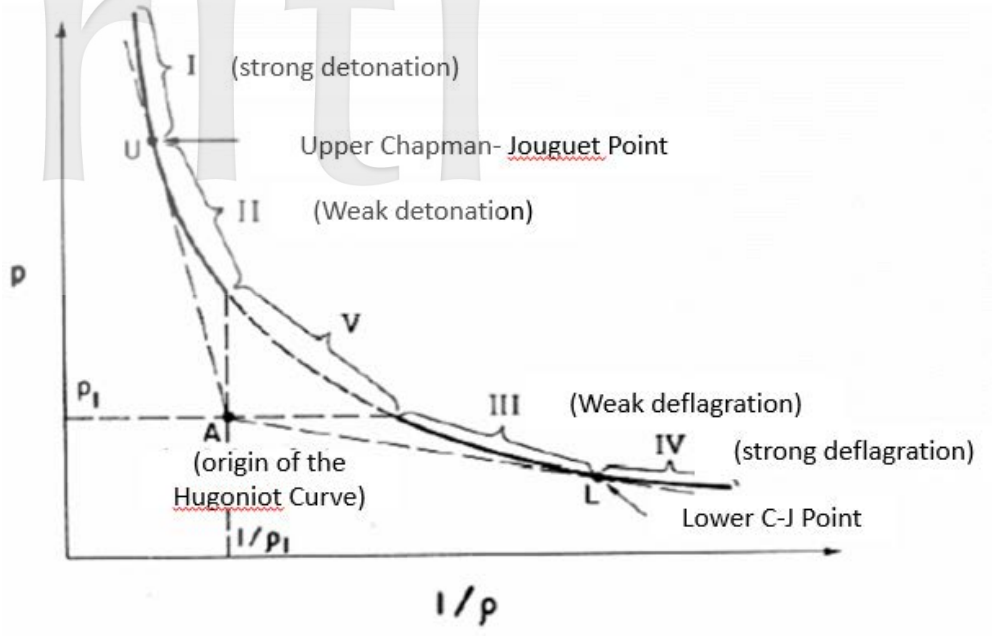

Figure 1 Rankine-Hugoniot Curve Describing Solutions of Combustion [13]

Based on Figure 1, Point A is the origin of the Rankine-Hugoniot Curve. This position is the initial state of the reactants ($1/\rho_1$, P_1Q). Tangents line through this origin and the curve form possible, stable solutions. Furthermore, the wave speed of the stable combustion wave (u_c) can be determined at the given tangent points, from the Rayleigh-line relation (Equation 1), and it can be deduced to:

$$u_c = \frac{1}{\rho_1}\left[\frac{P_2-P_1}{1/\rho_1 - 1/\rho_2}\right]^{\frac{1}{2}} \quad (3)$$

There are only four physically possible sections to the curve, namely Section I, II, III, and IV. Section I is the Strong Detonation section. This section represents overdriven detonations with pressures higher than that of a Chapman–Jouguet **(**CJ) detonation. These overdriven detonations are typically created at the onset of detonation and eventually stabilized to CJ detonation. Section II is the Weak Detonation section, which has a lower pressure than the CJ detonation. These weak detonation flames usually stabilize to a stable deflagration rather quickly and are rarely observed.

Section III and IV are the Weak and Strong Deflagration sections, respectively. In the Weak Deflagration section, the gas velocity accelerates from a subsonic velocity to a higher subsonic velocity as the gas passes through the combustion wave. However, in the Strong Deflagration section, the gas velocity must accelerate from a subsonic velocity to a significantly higher supersonic velocity. Unfortunately, in a constant area duct problem, the gas speed cannot be changed from subsonic to supersonic velocities due to the wave structures. Therefore, Weak Deflagrations are the most commonly observed form of deflagration combustion.

Ⅲ. BRAYTON AND HUMPHREY CYCLE

Figure 2(a) and 2(b) compare the pressure-specific volume and temperature-entropy characteristics of the Brayton and Humphrey cycles. The Brayton cycle represents the constant pressure heat addition of deflagration combustion, whereas the Humphrey cycles indicate the constant volume heat addition of the detonation combustion process [7]. The Brayton cycle (0-1-4-5-0) consists of two constant pressure processes (1-4 and 5-0) and two isentropic processes (0-1 and 4-5) [14]. The Humphrey cycle is similar, except that the constant pressure combustion process of the Brayton cycle, (1-4), is replaced by a constant volume heat addition process (1-2). The total area under the Humphrey P-v curve is higher than the total area under the Brayton P-v curve, indicating a much significant efficiency than the Humphrey cycle.

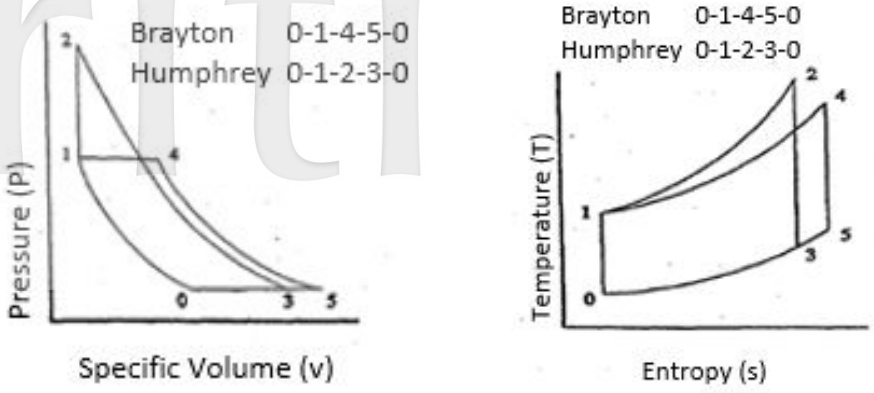

(a) (b)

Figure 2 (a) Pressure-Specific Volume Cycle Diagram (b) Temperature-Entropy Cycle Diagram [7]

The efficiencies of both the Brayton and Humphrey cycle are computable from the pressure-volume and temperature-entropy diagrams, as shown in Figure 2(a) and 2(b). The efficiency of a cycle can be defined as the useful work output divided by the total heat energy input. The efficiency of the Brayton cycle is based on the temperature change during either of the two isentropic compression or expansion processes (i.e., $T_0/T_1 = T_4/T_5$):

$$\eta_{BRAYTON} = 1 - \frac{T_0}{T_1} \quad (4)$$

The efficiency of the Humphrey cycle is as follows:

$$\eta_{HUMPHREY} = 1 - \gamma \frac{T_0}{T_1}\left[\frac{\left(\frac{T_2}{T_1}\right)^{\frac{1}{\gamma}}-1}{\frac{T_2}{T_1}-1}\right] \quad (5)$$

The difference between the Humphrey cycle and Brayton cycle is that although both cycles depend on the isentropic compression temperature ratio, T_0 / T_1, the Humphrey cycle relies on the ratio of specific heats, γ, and the temperature change due to the constant volume combustion (namely the detonation temperature ratio T_2/T_1). Therefore, the following multiplier is the main contributor to the differences between the Brayton and Humphrey cycle efficiencies:

$$\gamma \left[\frac{\left(\frac{T_2}{T_1}\right)^{\frac{1}{\gamma}}-1}{\frac{T_2}{T_1}-1}\right] \quad (6)$$

The value of this expression is always less than one for detonation combustion. As a result, the efficiency of a Humphrey (detonation) cycle is higher than the efficiency of the Brayton (deflagration) cycle.

IV. CYCLE ANALYSIS

Since the flow is one-dimensional and steady, the analysis is based on the equations of conservation for mass, momentum, and energy across the detonation, and the equation of state.

4.1 The Rayleigh Line

Simultaneous solution of mass and momentum conservation equations yields the following relationships:

$$\frac{P_2-P_1}{1/\rho_2-1/\rho_1} = -\dot{m}''^2 \quad (7)$$

The study uses the equation of state to get the Rayleigh Line by plotting P versus ν for a fixed flowrate. Then, it uses these generally linear relationships to plot a graph:

$$P = a\nu_2 + b \quad (8)$$

$$a = -\dot{m}''^2 \quad (9)$$

$$b = P_1 + \dot{m}''^2 \nu_1 \quad (10)$$

Figure 3 shows a plot of Rayleigh Line for State 1 fixed by P_1 and ν_1. By increasing the mass flux, $\dot{m}''^2$ causes the line to steepen, pivoting through the point (P_1, ν_1). The limit of infinite mass flux, the Rayleigh line is vertical, and the line becomes horizontal for the opposite limit of mass flux. Therefore, there is no possible solution in the quadrants labelled A and B.

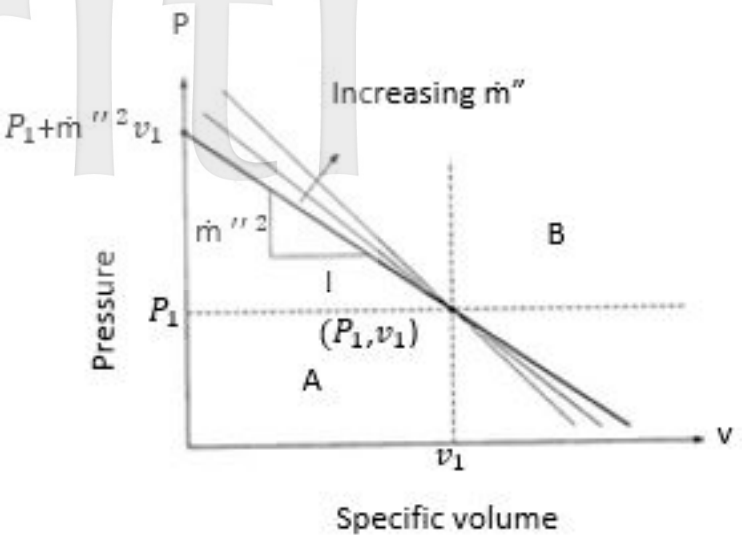

Figure 3 Bold line with slope $\dot{m}''^2$ is the Rayleigh line [3]

4.2 The Rankine-Hugoniot Curve

This curve can be obtained by combining mass, momentum and energy conservation and then employing the ideal-gas equation of state and other ideal-gas relations (e.g., $\gamma \equiv c_p/c_v$), which yields the following:

$$\frac{\gamma}{\gamma-1}(P_2 v_2 - P_1 v_1) - \frac{1}{2}(P_2 - P_1)(v_1 - v_2) - q = 0 \quad (11)$$

Then, the researchers plotted the pressure, P as a function of specific volume, v for P_1, v_1 and q fixed at mainly known values. The point (P_1, v_1) is sometimes referred to as the origin of the Rankine-Hugoniot curve. Figure 4 shows the Rankine-Hugoniot curve.

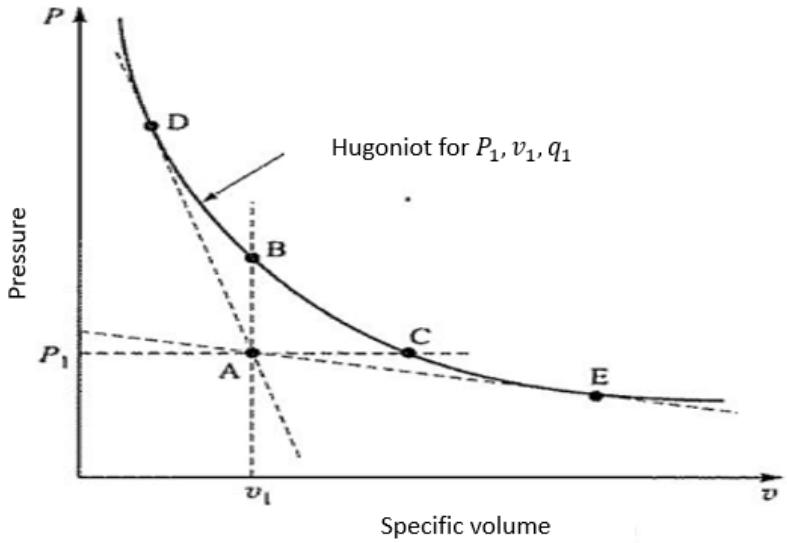

Figure 4 Rankine-Hugoniot curve for $q = q_1$ with origin A at (P_1, v_1) [3]

Essentially, to calculate Mach numbers, the researchers need to know both velocities and local sound speeds. The velocities are calculated from mass flux (Equation 10), ($\dot{m}'' = \rho_2 u_2 = u_2/v_2$) and ($c =$ speed of sound). Subsequently, to determine the speed of sound, they calculated the State-2 temperature from the ideal-gas equation and then computed the Mach number (for instance, in State-2):

$$M_2 = u_2/c_2 \quad (12)$$

V. DETONATION VELOCITIES

Detonation velocity, v_D, is defined as to be equal to the velocity at which the unburned mixture enters the detonation wave for an observer riding with the detonation. The expression is:

$$v_D \equiv u_1 \quad (13)$$

In determining the velocities of detonation, the researchers need to add one more assumption, which is the pressure of the burned gases is higher than the pressure of the unburned mixture, $P_2 \gg P_1$. As the detonation occurs at State-2, which is the upper Chapman-Jouguet point where the gas velocity is sonic, the researchers rewrite the mass conservation as:

$$\rho_1 u_1 = \rho_2 c_2 \quad (14)$$

Then, by solving u_1 and substituting $c_2 = (\gamma R_2 T_2)^{1/2}$ into Equation 14, they yield:

$$u_1 = \frac{\rho_2}{\rho_1}(\gamma R_2 T_2)^{1/2} \quad (15)$$

Subsequently, the researchers relate the density ratio, ρ_2/ρ_1 and T_2 to the upstream or other known quantities. The study then finds the expression for ρ_2/ρ_1, which starts with mass conservation and divides it by ρ_2/u_2^2. Then, by neglecting P_1, the study yields the following:

$$\frac{\rho_1 u_1^2}{\rho_2 u_2^2} - \frac{P_2}{\rho_2 u_2^2} \quad (16)$$

Next, the researchers apply mass conservation and simplify the equation. They then replace u_2^2 with $c_2^2 = \gamma R_2 T_2$ and simplifies it with the ideal gas law, $P_2 = \rho_2 R_2 T_2$:

$$\frac{\rho_2}{\rho_1} = 1 + \frac{1}{\gamma} \quad (17)$$

In the next step, the researchers relate T_2 with known quantities by solving the energy conservation for T_2 and simplifies the equation. They replace u_2^2 with $c_2^2 = \gamma R_2 T_2$:

$$T_2 = T_1 + + \frac{q}{c_p} + \frac{\gamma R_2 T_2}{2c_p}\left[\left(\frac{\gamma+1}{\gamma}\right)^2 - 1\right] \quad (18)$$

Hence, solving (Equation 18) for T_2 results in:

$$T_2 = \frac{2\gamma^2}{\gamma+1}\left(T_1 + \frac{q}{c_p}\right) \quad (19)$$

To determine v_D, the researchers then substitute Equation 17 and Equation 19 into Equation 15 to yield:

$$v_D = u_1 = \left[2(\gamma+1)\gamma R_2(T_1 + q/c_p)\right]^{1/2} \quad (20)$$

Equation 20 is approximate, not only because of the approximations employed in specifying the physics but also because of the numerical approximation that $P_2 \gg P_1$. Then, the assumption of constant and equal specific heats, the expression for the State-2 temperature and the detonation velocity can be derived as:

$$T_2 = \frac{2\gamma_2^2}{\gamma_2+1}\left(\frac{c_{p,1}}{c_{p,2}}T_1 + \frac{q}{c_{p,2}}\right) \quad (21)$$

$$v_D = \left[2(\gamma_2+1)\gamma_2 R_2\left(\frac{c_{p,1}}{c_{p,2}}T_1 + q/c_{p,2}\right)\right]^{1/2} \quad (22)$$

Where $c_{p,1}$ and $c_{p,2}$ are a mixture of specific heats at States 1 and 2, respectively.

VI. PERFORMANCE ANALYSIS

This section develops mathematical expressions for the performance characteristics of PDE. Based on the ideal supersonic heat addition PDE T-s diagram in Figure 5, the flow at the inlet from Station 0 to Station 2 is at supersonic Mach number ($M_2 > 1$), next to Station 2 to Station 4 with the Mach number at Station 4 ($M_4 = 1$) being sonic. The process from Station 2 to Station 4 is controlled by the Chapman-Jouguet condition, which requires a sonic Mach number at the end of the heat addition (Station 4). The freestream flow condition (τ_r), the diffuser compression (τ_2) and the added heat (T_{max}) determine the strength of the leading shock wave from Station 2 to Station 2a. The process from Station 4 to Station 9 is an ideal exit nozzle isentropic expansion to the freestream ambient pressure.

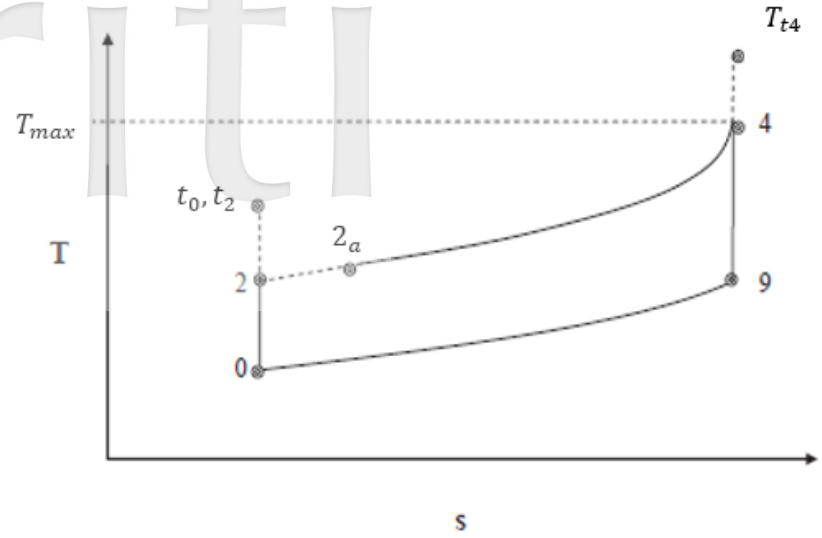

Figure 5 Ideal Supersonic Heat Addition PDE T-s Diagram [15]

6.1 Chapmen-Jouguet Mach Number

The algebraic solution for the leading normal shock wave (Chapman–Jouguet) Mach number is developed and in compliance with Figure 4, which is given by:

$$M_{CJ}^2 = \left\{(\gamma+1)\frac{\bar{q}}{\psi}+1\right\} + \sqrt{\left\{(\gamma+1)\frac{\bar{q}}{\psi}+1\right\}^2 - 1} \quad (23)$$

$$\bar{q} = \frac{f.h_{PR}}{c_p T_0} \quad (24)$$

$$\psi = \frac{T_2}{T_0} = \frac{T_2}{T_{t2}}\frac{T_{t2}}{T_0} = \frac{\tau_r}{\tau_2} \quad (25)$$

$$M_{CJ}^2 = \left\{(\gamma+1)\frac{[\tau_\lambda - \tau_r]}{\tau_r/\tau_2}+1\right\} + \sqrt{\left\{\frac{(\gamma+1)}{\tau_r/\tau_2}[\tau_\lambda - \tau_r]+1\right\}^2 - 1} \quad (28)$$

$$\tau_r = [1 + (\gamma-1)\,M_0^2/2] \quad (29)$$

$$\tau_2 = [1 + (\gamma-1)\,M_2^2/2] \quad (30)$$

Where M_0 and M_2 are the parameters to be selected. Equation 28 shows that M_{cj} is determined by specifying the diffuser temperature ratio, τ_2, the freestream conditions, τ_r (M_0, T_0), and the burner outlet total temperature $\tau_\lambda(T_{t4})$, where T_{t4} is a function of T_{max}, $T_{t4}(T_{max})$; the expression for T_{t4} as a function of T_{max} is developed later in this section; T_{max} is the maximum temperature limit.

6.2 Thermal Efficiency

The study derives the entropy rise in the detonation wave as:

$$\frac{s_4 - s_2}{c_p} = -\ln\left\{M_{CJ}^2\left(\frac{\gamma+1}{1+\gamma M_{CJ}^2}\right)^{\frac{\gamma+1}{\gamma}}\right\} \quad (31)$$

Note that the entropy change from 0 to 9 in Figure 4 is the same as the entropy change from 2 to 4 and is exemplified by:

By employing the first law of thermodynamics across the combustion chamber, the expression for the fuel-to-air ratio is given by:

$$f = \frac{c_p T_0}{h_{PR}}(\tau_\lambda - \tau_r) \quad (26)$$

$$\tau_\lambda = T_{t4}/T_0 \quad (27)$$

The substitution of Equation 24, Equation 25 and Equation 26 into Equation 23 yields:

$$\frac{s_9 - s_0}{c_p} = \ln\left\{\left(\frac{T_9/T_0}{\left(\frac{P_9}{P_0}\right)^{\frac{\gamma-1}{\gamma}}}\right)\right\} \quad (32)$$

But $P_9/P_0 = 1$, thus:

$$T_9/T_0 = \exp\left\{\frac{s_9 - s_0}{c_p}\right\} = \exp\left\{\frac{s_4 - s_2}{c_p}\right\} \quad (33)$$

Then, note that:

$$q_{out} = c_p T_0\left[\frac{T_9}{T_0} - 1\right] \quad (34)$$

$$q_{in} = f.h_{PR} \quad (35)$$

The researchers insert Equation 31 into Equation 33 to obtain an expression for T_9/T_0 and then by inserting the expression for T_9/T_0 into Equation 34, they yield:

$$q_{out} = c_p T_0\left[\frac{1}{M_{CJ}^2}\left(\frac{1+\gamma M_{CJ}^2}{\gamma+1}\right)^{\frac{\gamma+1}{\gamma}} - 1\right] \quad (36)$$

The next step is inserting Equation 35 and Equation 36 into Equation 49:

$$\eta_T = \frac{Q_{in}-Q_{out}}{Q_{out}} = 1 - \frac{q_{out}}{q_{in}} \quad (37)$$

$$\eta_T = 1 - \frac{\left\{\frac{1}{M_{CJ}^2}\left(\frac{1+\gamma M_{CJ}^2}{\gamma+1}\right)^{\frac{\gamma+1}{\gamma}} - 1\right\}}{[\tau_\lambda - \tau_r]} \quad (38)$$

Hence, the thermal efficiency is a function of T_0, M_0, M_2 and $T_{t4}(T_{max})$, and is under the following expression:

$$\eta_T = \frac{\dot{w}_{out}}{q_{in}} = \frac{(V_9^2 - V_0^2)/2}{f.h_{PR}} \quad (39)$$

6.3 Thrust-specific Fuel Consumption and Propulsive Efficiency

First, by solving Equation 39 for V_9, they yield:

$$V_9 = \sqrt{V_0^2 + 2\eta_T.f.h_{PR}} \quad (40)$$

The expression for the specific thrust is:

$$\frac{F}{\dot{m}_o} = \frac{1}{g_c}[V_9 - V_0] \quad (41)$$

The substitution of Equation 40 in Equation 41 gets:

$$\frac{F}{\dot{m}_o} = \frac{1}{g_c}[\sqrt{V_0^2 + 2\eta_T.f.h_{PR}} - V_0] \quad (42)$$

Next, the researchers multiply and divide the right side of Equation 42 by a freestream speed of sound, a_0, and with a simple algebra for an ideal gas, they yield:

$$\frac{F}{\dot{m}_o} = \frac{a_0}{g_c}\left[\sqrt{M_0^2 + \frac{2}{(\gamma-1)}(\tau_\lambda - \tau_r)\eta_T} - M_0\right] \quad (43)$$

The study expressed thrust-specific fuel consumption as:

$$S = \frac{f}{F/\dot{m}_o} \quad (44)$$

The substitution of Equation 26 and Equation 43 into Equation 44, yields:

$$S = \frac{(\tau_\lambda - \tau_r)(c_p T_0/h_{PR})}{\frac{a_0}{g_c}\left[\sqrt{M_0^2 + \frac{2}{(\gamma-1)}(\tau_\lambda - \tau_r)\eta_T} - M_0\right]} \quad (45)$$

$$\eta_P = \frac{2}{\sqrt{1 + \frac{2}{(\gamma-1)M_0^2}\frac{\eta_T}{(\tau_\lambda - \tau_r)} + 1}} \quad (46)$$

Finally, the overall efficiency:

$$\eta_0 = \eta_P \eta_T \quad (47)$$

VII. RESULTS AND DISCUSSION

7.1 Thermodynamics Condition under Detonation Combustion

Initially, this study calculates the thermodynamic properties of each fuel before the parametric analysis of fuel comparison under detonation combustion. The study begins by obtaining the fundamental properties and conditions of fuels, such as the mass flux, initial temperature, specific heat ratio, and specific heat constant. Table 2 shows the properties of the analyzed fuels in this report. The study had to go through several steps to determine that the fuels underwent detonation combustion, which varied either in the mass flux or initial temperature. Then, with the respective values of each property, the study compared the fuels to obtain the pressure, temperature, density, and Mach number ratios.

Table 2 Thermochemical Properties and Initial Condition of Fuels

	Babassu Biokerosene BBK100 $C_{12.18}H_{24.36}O_2$	Bioethanol C_2H_5OH	Hydrogen gas H_2
$\dot{m}^{"}$	2800	2800	4400
T_1	360	380	550
c_{p1}	0.946	1.071	0.701
γ_1	1.396	1.350	1.4

Table 2 indicates that the Babassu Biokerosene fuel is the easiest to detonate among the others, where it has the lowest minimum temperature, $T_{1,}$ and mass flux, $\dot{m}^{"}$. The study also observed that as the initial temperature varies, the mass flux was constant at $2500\ kg/sm^{-2}$ and when the mass flux varies, the initial temperature was constant at 300K. In contrast, the hydrogen gas fuel was the most difficult to detonate, where it required a high temperature and mass flux.

7.2 Varying Initial Parameters of Fuels

This study analyzed the comparison of fuels in terms of temperature, pressure, density, and Mach number ratios and the result corresponds with the varying initial parameters of fuels. These ratios represent the ratio of unburn gas against burned gas.

7.2.1 Various Mass Flux

When varying the mass flux, the researchers kept the initial temperature constant at 300K. The mass flux varied from $3500\,kg/sm^{-2}$ to $9400\,kg/sm^{-2}$. The study then utilized mathematical modelling by combining the cycle analysis in a one-dimensional to compare the properties of the fuel, and the result was the plot in the graph. As plotted in Figure 6, conclusively, the trend for all fuels is the same — nevertheless, values between fuels differ based on different ratios. In Figure 6(a) and Figure 6(b), as the mass flux increases, the temperature ratio and pressure ratio also increase. Meanwhile, Figure 6(c) depicts a steady increase. In Figure 6(d), the ratio of Mach number for hydrogen gas is higher than both types of biofuels.

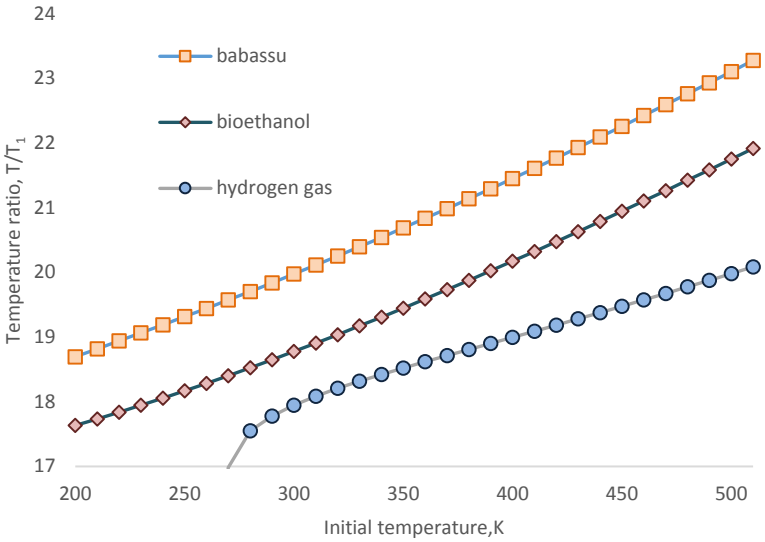

(a)

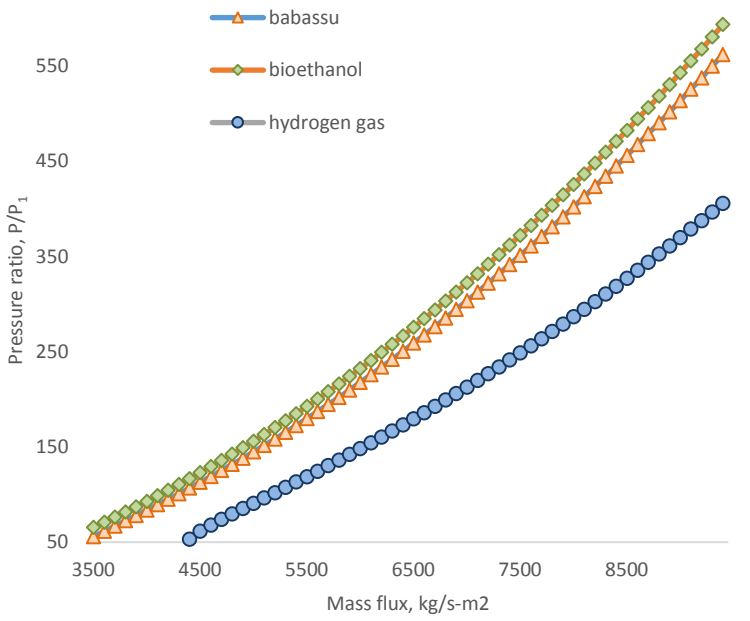

(b)

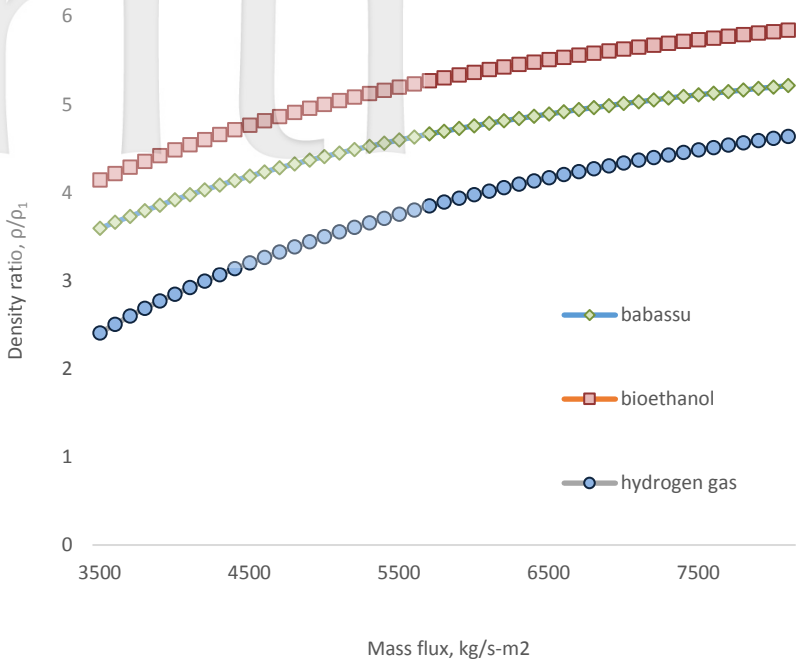

(c)

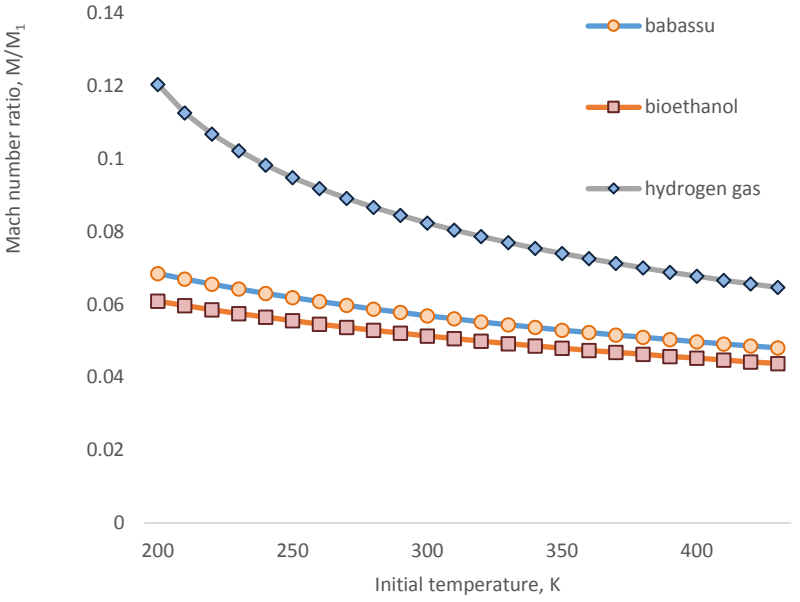

(d)

Figure 6 (a) Temperature Ratio (b) Pressure Ratio (c) Density Ratio (d) Mach Number Ratio for Various Mass Flux

7.2.2 Various Initial Temperature

The initial temperature varied from 200K to 790K, while the mass flux was constant at 2500. Figure 7(a) indicates that as the initial temperature increases, so did the temperature ratio. Biofuel Babassu Biokerosene BBK100 has the highest temperature ratio at every point. The trend for both pressure and density ratios are the same for all fuels, but the difference is the values of the ratio. Then again, Figure 7(d) indicates that both Babassu and Bioethanol do not have much difference in their trend of line.

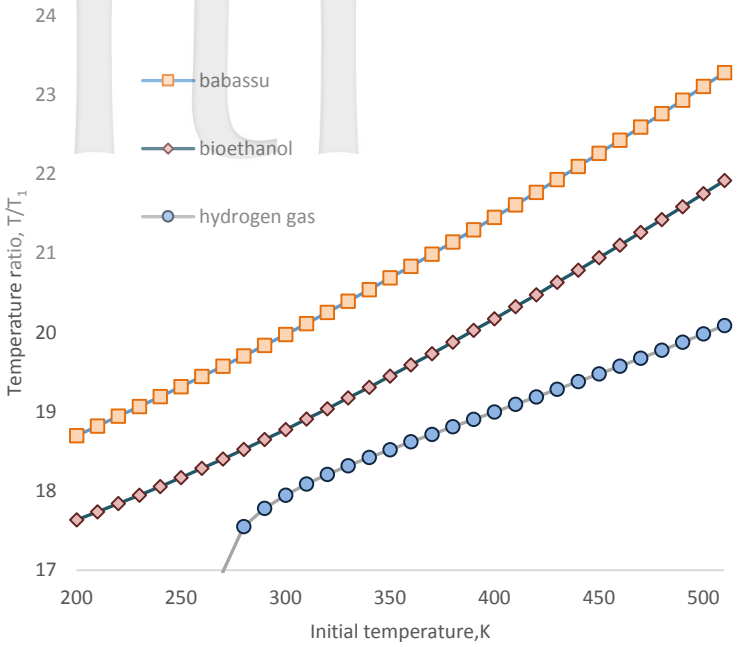
babassu
bioethanol
hydrogen gas
Temperature ratio, T/T1
Initial temperature,K
24
23
22
21
20
19
18
17
200
250
300
350
400
450
500

(a)

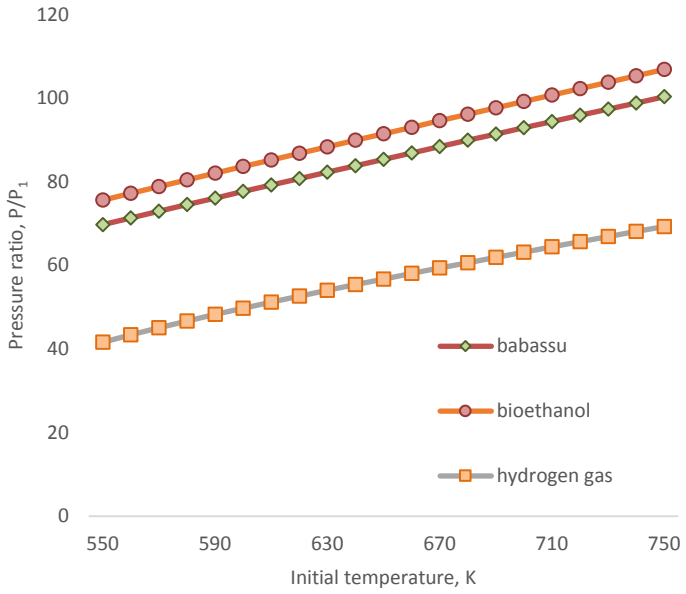
babassu
bioethanol
hydrogen gas
Pressure ratio, P/P1
Initial temperature, K
120
100
80
60
40
20
0
550
590
630
670
710
750

(b)

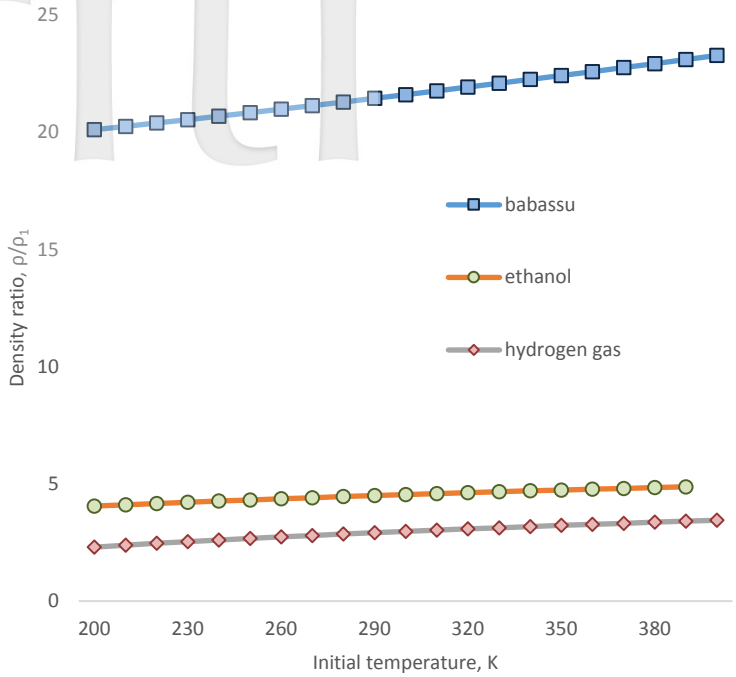

(c)

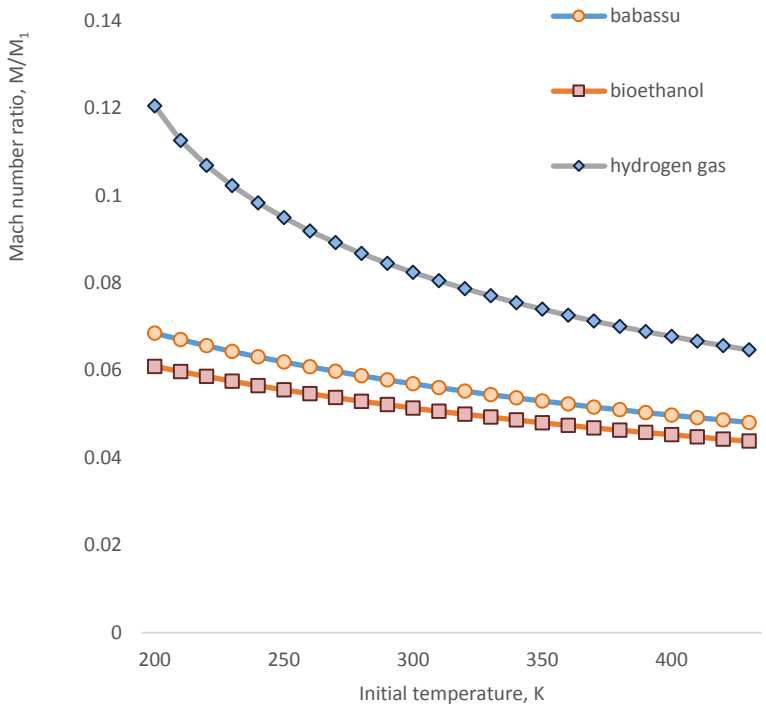

(d)

Figure 7 (a) Temperature Ratio (b) Pressure Ratio (c) Density Ratio (d) Mach Number for Various Initial Temperature

7.3 Detonation Velocity

The estimation of detonation velocity started with the finding of all initial parameters of unburned gas. The study considered the fuels under stoichiometric combustion; hence, they need to apply the balancing of the unreacted, and the reacted mixture before calculating through mathematical modelling. Table 3 represents the detonation velocity of fuels under detonation combustion. Based on Table 3, hydrogen gas has higher detonation velocity as it is in a gas state, but if compared to both types of biofuels, Babassu has a higher detonation velocity than Bioethanol due to the thermodynamic properties of Babassu.

Table 3 Detonation velocity at (P=1atm, T=300K)

	Babassu BBK100	Bioethanol	Hydrogen gas
V_D	1900.4	1758.9	5474.1

7.4 Performance Analysis

7.4.1 Validation of Parametric Cycle of PDE

This research identified the performance characteristic through the parametric cycle of an ideal Pulse Detonation Engine. This parametric cycle has function freestream Mach number, M_0 and Mach number at combustor inlet, M_2 is taken as various parameters. M_2 varies at $M_2 = 1.1$, $M_2 = 2$, $M_2 = 3$ and $M_2 = 4$. This section analyses the comparison of biofuels with conventional Kerosene under the ideal supersonic heat addition of PDE. The initial parameters were in the forms of $T_0 = 298K$, $T_{max} = 1666K$, h_{PR} and $c_p = 1.004kJ/kgmol$.

7.4.2 Thermal Efficiency

Based on Figure 8, the conventional Kerosene has a slightly higher thermal efficiency, η_T than Bioethanol. Nevertheless, Babassu's thermal efficiency is the same as Kerosene. Therefore, the graph shows that thermal efficiency increases as M_o increases.

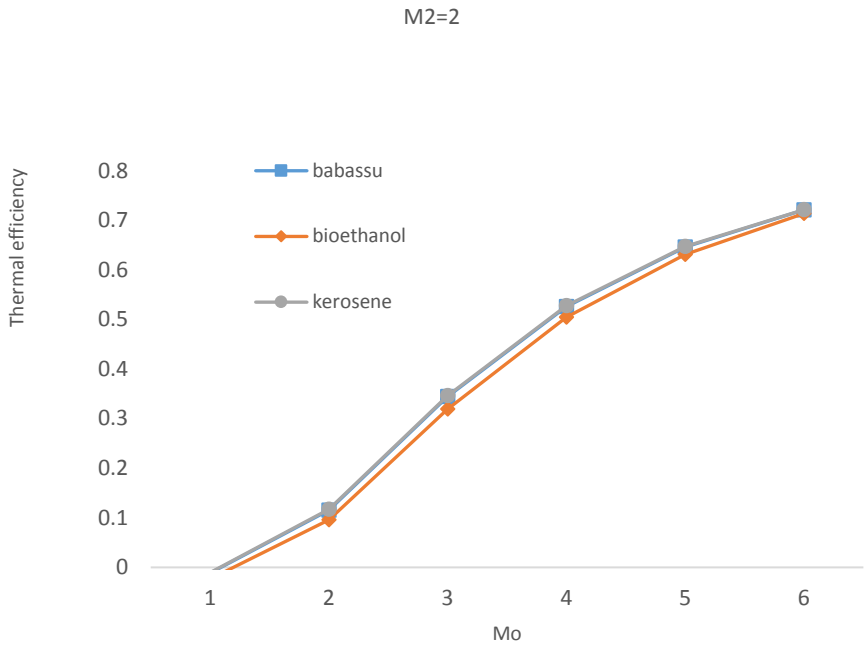

(a) $M_2 = 2$

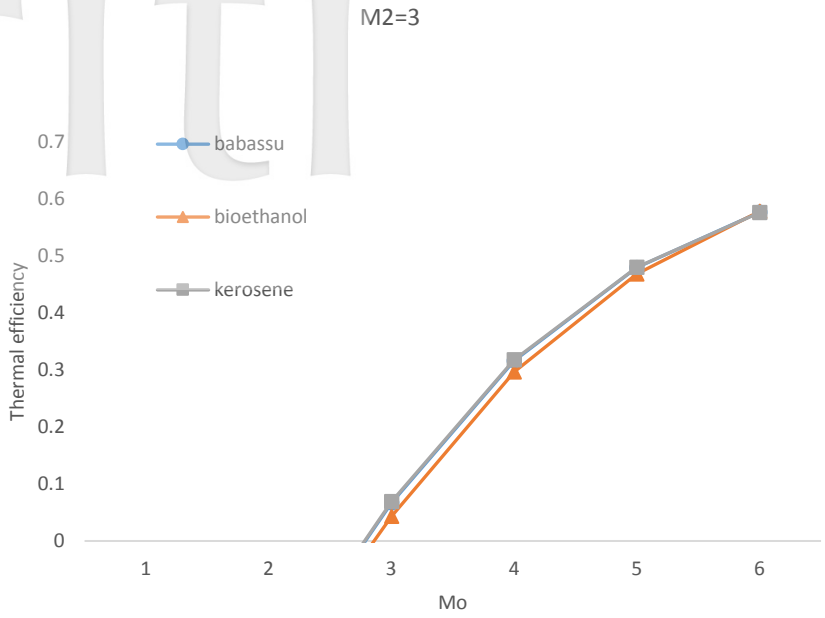

(b) $M_2 = 3$

Figure 8 Freestream Mach Number, M_o vs Thermal Efficiency, η_T

7.4.3 Propulsive Efficiency and Overall Efficiency

Before calculating propulsive efficiency, η_p, it was necessary to analyse the fuel-to-air ratio. Hence, Figure 9 shows the fuel-to-air ratio versus M_o. Bioethanol and Babassu have a higher fuel-to-air ratio than Kerosene. The trend of the graph is the same for all fuels; as freestream Mach number increases, the fuel-to-air ratio decreases.

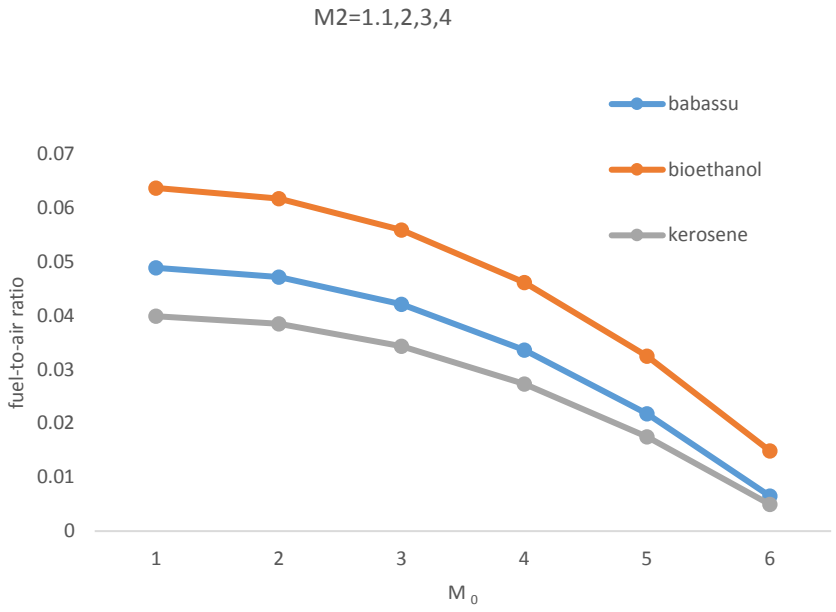

Figure 9 Freestream Mach Number, M_o vs Fuel-to-air Ratio, f

Figure 10 illustrates the propulsive efficiency as function freestream Mach number. In brief, under PDE, both fuels; conventional and biofuels generate almost the same magnitude of propulsive efficiency.

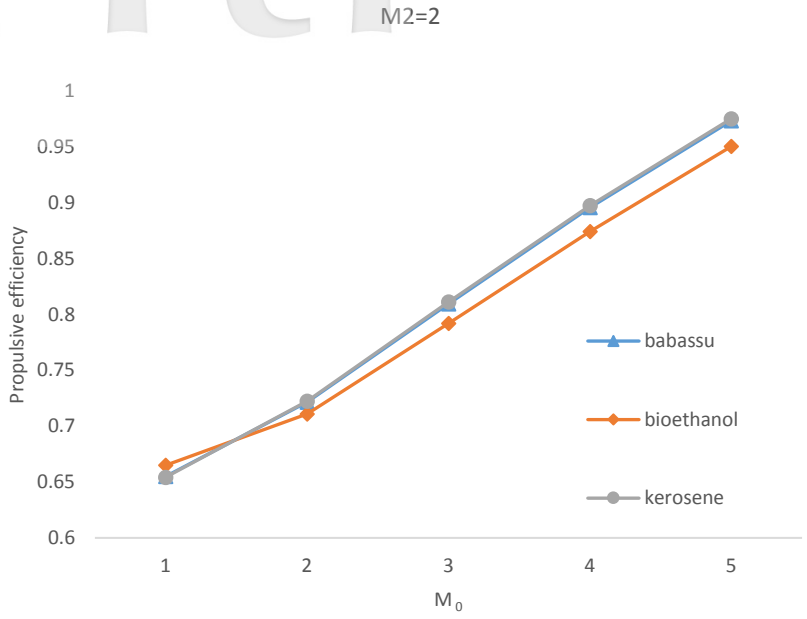

(a) $M_2 = 2$

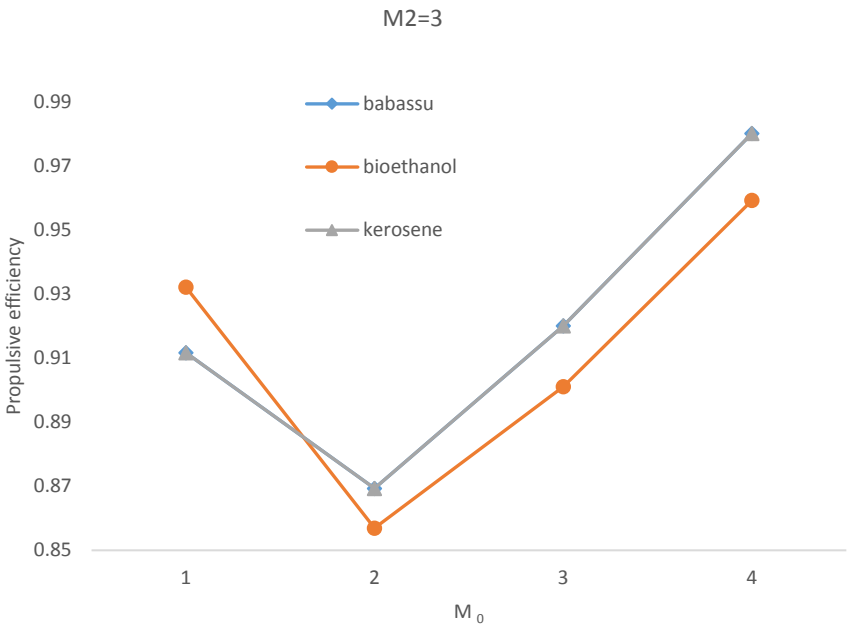

(b) $M_2 = 3$

Figure 10 Freestream Mach number, M_o vs Propulsive Efficiency, η_P

The overall efficiency of Bioethanol is slightly below the Kerosene Babassu. At a certain point in freestream Mach number, both Kerosene and Babassu are more efficient than Bioethanol. Due to the high thermodynamic properties of Babassu in comparison to Bioethanol, the final value of efficiency differs.

(a) $M_2 = 2$

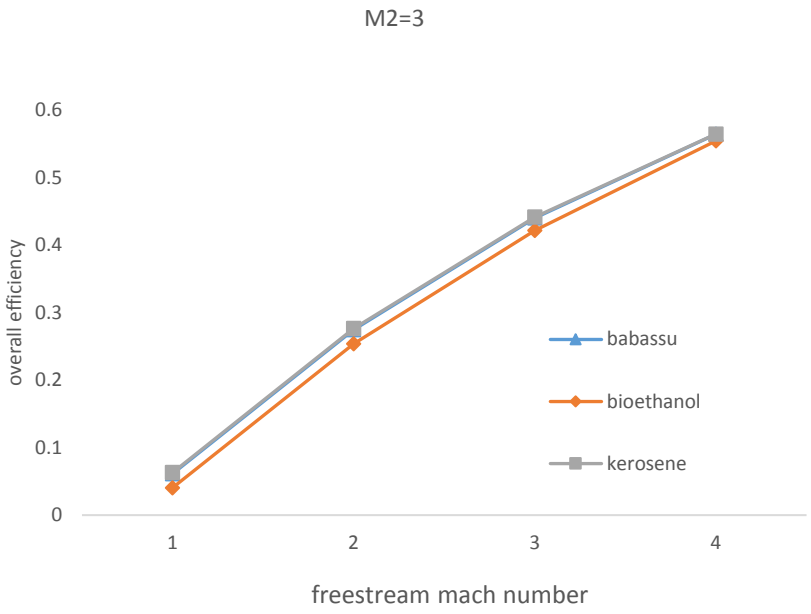

(b) $M_2 = 3$

Figure 11 Freestream Mach Number, M_o vs Overall Efficiency, η_0

7.4.4 Various Combustor Entrance Mach Number

Subsequently, the study sets the M_2 parameters to specific values of which were $M_2 = 1.1$, $M_2 = 2$, $M_2 = 3$ and $M_2 = 4$. This time, the study only analyses one type of fuel, and in this section, the study models and differentiates the combustor entrance Mach number, M_2 and the effect of the ideal PDE performance. Figure 12(a) shows the $M_o vs\ M_{CJ}$ of Babassu which indicates that at an early stage of M_o, there is a large gap between M_{CJ} because of the difference in M_2. In M_2, the parameter is equal to 1.1, $M_{CJ} = 6$ whereas at $M_2 = 4$, M_{CJ} is more than 10. The thermal efficiency of Babassu drops when M_2 is higher. As indicated in Figure 12(c), as the freestream Mach number M_o increases, the propulsive efficiency becomes steadily either a different value of M_2, or the propulsive efficiency becomes almost 1. Lastly, the overall efficiency becomes higher, when the combustor entrance Mach number reduces to $M_2 = 1$.

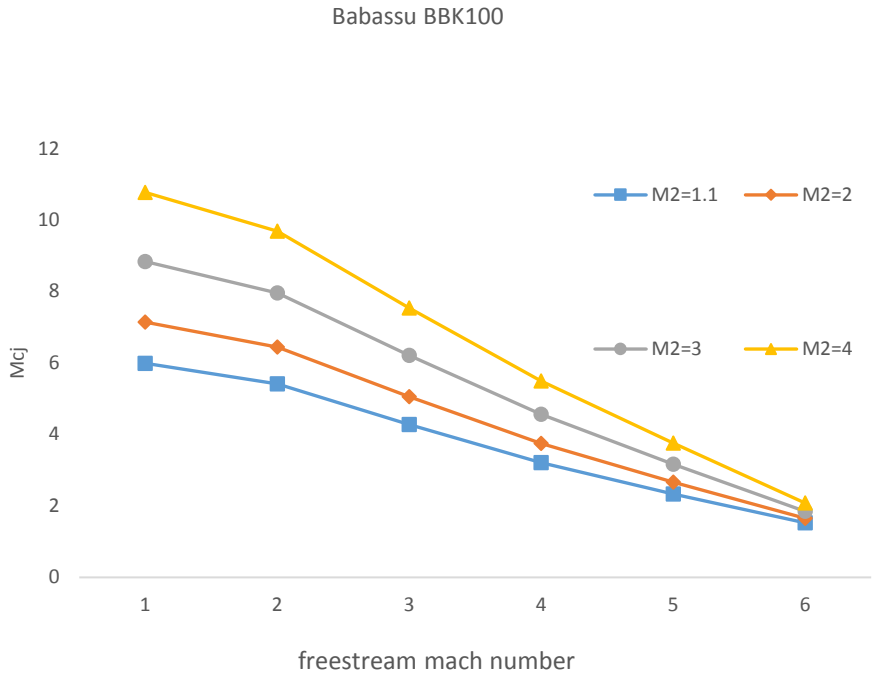

(a) M_o vs M_{CJ}

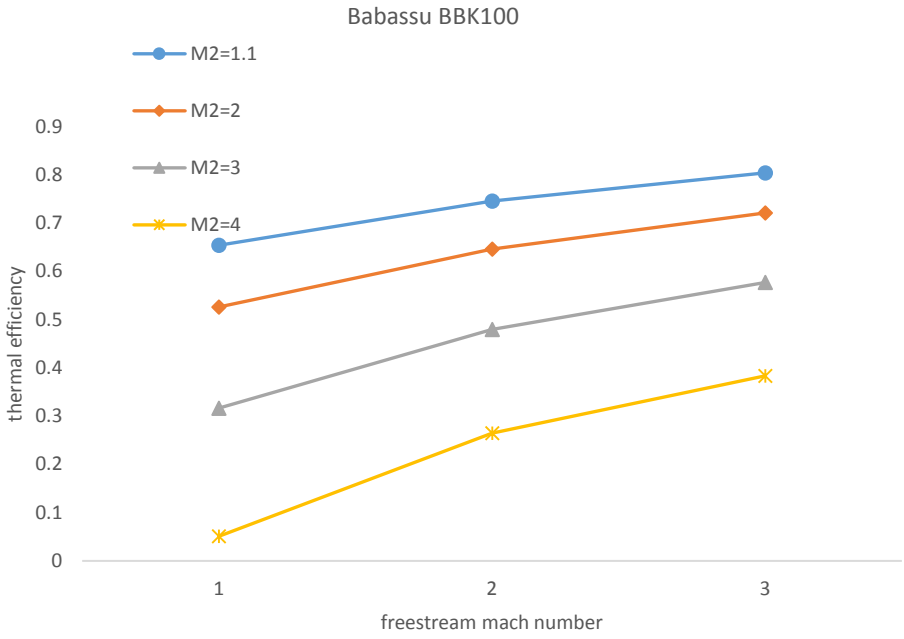

(b) M_o vs η_T

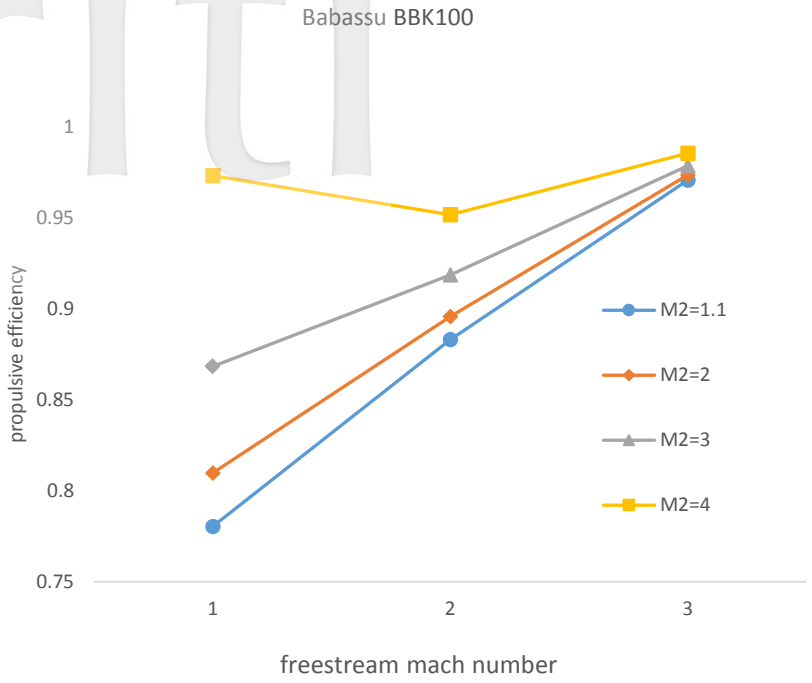

(c) $M_o$vs η_P

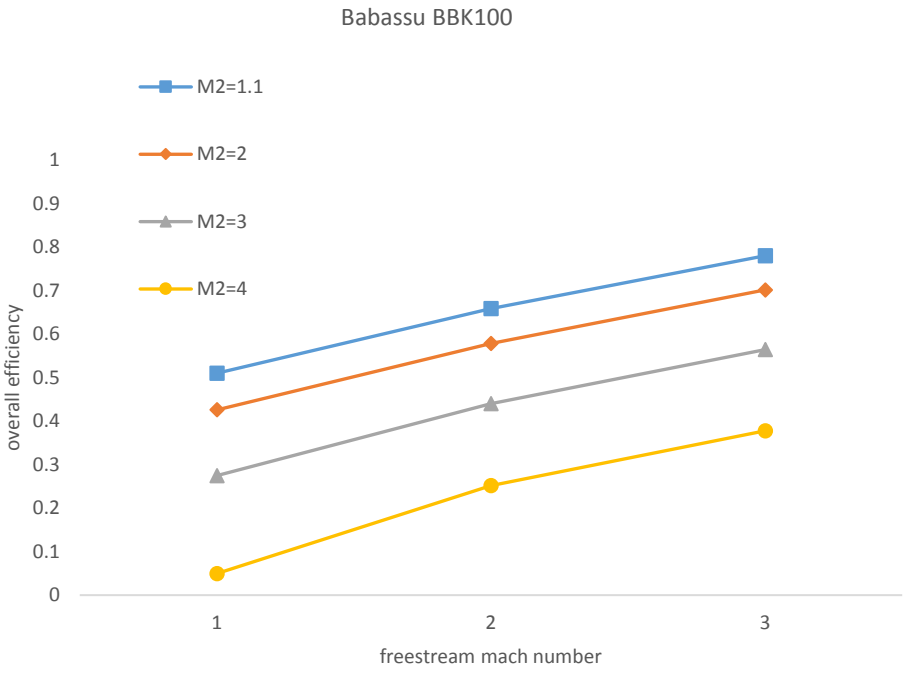

(d) $M_o vs\ \eta_o$

Figure 12 Freestream Mach number, M_o vs Performance

VIII. CONCLUSION

In this report, the researchers completed the parametric analysis of the performance of an ideal Pulse Detonation Engine (PDE) and the assessment of Biofuel on thermophysical and propulsive performance under PDE. The study made a comparison of biofuels properties as alternative fuels by analyzing through mathematical modelling to check the feasibility and effectiveness. Initially, the researchers selected four different types of

fuel and two were biofuels, Babassu BBK100 and Bioethanol, ideal-gas Hydrogen gas, and Kerosene, a type of fossil fuel. The analysis starts with the application of an algebraic expression that is related to the one-dimensional detonation combustion process, such as the Rayleigh line, Rankine-Hugoniot Curve, and ZND model [16]. The comparison of the fuels' properties is of temperature, pressure, density, and Mach number ratios by varying the initial temperature and mass flux of the reactant or unburn gas. Then, the primary conditions of the biofuels confirmed whether they are feasible for PDEs. This study analyzed the detonation velocity based on the state of the fuels' properties in reactants and the product chemical reaction of stoichiometric combustion. Once the detonation velocity is acquired, the researchers are then able to classify the fuels. The study deduced that Babassu has a higher detonation velocity compared to Bioethanol, which is 1900.4 and 1758.9, respectively.

The first part of this research compares Babassu, Bioethanol, and Hydrogen gas. The second part models the propulsive performance of biofuels with Kerosene that acts as a benchmark. Consequently, the performance analysis shows that Babassu is much efficient to work under detonation combustion, yet Bioethanol can also perform in PDE. The result of this study shows that Babbassu can function as an alternative fuel in the propulsion system. Apart from its effectiveness in the detonation combustion process, Babassu also reduces the effects of pollution in the environment.

ACKNOWLEDGEMENT

The authors would like to thank and acknowledge the Ministry of Education for the Fundamental Research Grant Scheme (FRGS19-063-0671) in completing this research.

REFERENCES

[1] Paxson DE, "Numerical Analysis of a Rotating Detonation Engine in the Relative Reference Frame," *AIAA SciTech*, Vol. 1, No. January 2014, pp. 1–14.

[2] Lu FK, Braun EM, "Rotating Detonation Wave Propulsion: Experimental Challenges, Modeling, and Engine Concepts," *Journal Propuls. Power*, Vol. 30, No. 5, 2014, pp. 1125–1142.

[3] Turn SR, Introduction to Combustion: concept and application. 2000.

[4] Pandey KM, Debnath P, "Review on Recent Advances in Pulse Detonation Engines," *Journal Combust*, Vol. 1, No. 1, 2016, pp. 1–16.

[5] Eidelman S, Grossmann W, Lottati I, "Review of Propulsion Applications and Numerical Simulations of the Pulsed Detonation Engine Concept," *Journal Propuls*, Vol. 7, No. 6, 1991.

[6] Ma F, Choi J, Yang V, "Thrust Chamber Dynamics and Propulsive Performance of Multitube Pulse Detonation Engines," Vol. 21, No. 4, 2005.

[7] Coleman ML, "Overview of Pulse Detonation Propulsion Technology," *Chemical Propulsion Information Agency*, Vol. 1, No. April 2001, pp. 1–64.

[8] Lefkowitz JK et al., "Schlieren imaging and pulsed detBussing, T., & Pappas, G. (1994). An Introduction to Pulse Detonation Engine. AIAA Journal, 1–15. Detonation engine testing of ignition by a nanosecond repetitively pulsed discharge," *Combust. Flame*, Vol. 1, No. 1, 2015, pp. 1–12.

[9] Smirnov NN, Betelin VB, Nikitin VF, Phylippov YG, Koo J, "Detonation engine fed by acetylene – oxygen mixture," *Acta Astronaut*, Vol. 104, No. 1, 2014, pp. 134–146.

[10] Wolanski P, "Detonation engines," *Journal of KONES Powertrain and Transport*, Vol. 18, No. 3, 2011, pp. 515–521.

[11] Azami MH, Savill M, "Comparative Analysis of Alternative Fuels in Detonation Combustion," *Propuls. Energy Forum*, Vol. 1, No. 1, 2016, pp. 1–17.

[12] Singh A, Singh P, Murphy JD, "Renewable fuels from algae: An answer to debatable land-based fuels," *Bioresour. Technol*, Vol. 102, No. 1, 2011, pp. 10–16.

[13] Bussing T, Pappas G, "An Introduction to Pulse Detonation Engine," *AIAA Journal*, pp. 1–15, 1994.

[14] Frolov SM, Aksenov VS, Ivanov VS, Shamshin IO, "Thrust Characteristics of a Pulse Detonation Engine Operating on a Liquid Hydrocarbon Fuel," *Russian Journal of Physical Chemistry*, Vol. 10, No. 2, 2016, pp. 291–292.

[15] Roux JA, "Parametric cycle analysis of an ideal pulse detonation engine – Supersonic branch," *Thermal Science and Engineering Progress*, Vol. 5, 2018, pp. 296–302.

[16] Azami MH, Savill M, "Pulse Detonation Assessment for Alternative Fuels," *Energy*, Vol. 10, pp. 1–19, 2017.